Defect modes in imperfect periodic structures

Yilun Li, Régis Cottereau, Bing Tie

▶ **To cite this version:**

Yilun Li, Régis Cottereau, Bing Tie. Defect modes in imperfect periodic structures. Journal of Physics: Conference Series, 2024. hal-04516732

HAL Id: hal-04516732
https://hal.science/hal-04516732

Submitted on 22 Mar 2024

HAL is a multi-disciplinary open access archive for the deposit and dissemination of scientific research documents, whether they are published or not. The documents may come from teaching and research institutions in France or abroad, or from public or private research centers.

L'archive ouverte pluridisciplinaire **HAL**, est destinée au dépôt et à la diffusion de documents scientifiques de niveau recherche, publiés ou non, émanant des établissements d'enseignement et de recherche français ou étrangers, des laboratoires publics ou privés.

Defect modes in imperfect periodic structures

Yilun Li[1], Régis Cottereau[2] and Bing Tie[1]

[1] Université Paris-Saclay, CentraleSupélec, ENS Paris-Saclay, CNRS, LMPS, Gif-Sur-Yvette, 91190, France

[2] Aix-Marseille Université, CNRS, Centrale Marseille, LMA UMR 7031, Marseille, France

E-mail: yilun.li@centralesupelec.fr, cottereau@lma.cnrs-mrs.fr, bing.tie@centralesupelec.fr

Abstract. Lack of periodicity in engineering structures can arise because of imperfections in the production process or a particular purpose to produce desirable physical effects. This contribution presents a series of numerical simulations that quantitatively characterize the influence of defects on the dispersion relation and associated eigenmodes of imperfect periodic structures. Local defects are introduced periodically on a scale larger than the size of the unit cell of the non-disturbed periodic structure. The observations reveal that these defects can give rise to non-propagating modes at frequencies situated within the bandgaps of the periodic structure. The eigenfrequency of such a defect mode varies monotonically with the amplitude of the defects, and its deformations are located in and around the disturbed cell. Furthermore, a bounded periodic medium with defects is studied by finite element analysis to demonstrate the existence of these defect modes in bounded imperfect periodic structures.

1. Introduction

Periodic structures offer unique advantages in the realm of wave propagation, with features like negative refractive index, frequency band gaps for effective wave filtration, and efficient vibration isolation. These distinctive properties have propelled the widespread adoption and rapid expansion of periodic structures, finding applications in metamaterials [1–6] and phononic crystals [7–11]. The investigation of wave propagation behaviors in periodic systems can be reduced to that of a unit cell through the use of Floquet-Bloch analysis [12–17]. However, Lack of periodicity in engineering structures can arise because of imperfections in the production process [18–24] and potentially undermining the favorable traits highlighted earlier [25, 26]. It is also possible to deliberately disrupt periodicity for a particular purpose to produce desirable physical effects. In both cases, understanding the effects of periodicity defects on wave propagation phenomena is crucial and requires thorough investigation.

In this paper, we present a series of numerical simulations that quantitatively characterize the influence of defects on the dispersion relation and associated eigenmodes of imperfect periodic structures. Localized defects are introduced periodically on a larger scale than that of the unit cell of the non-disturbed periodic structure. The wave propagation in such periodic media with various defects of mechanical or geometric properties is analyzed and compared to the reference case without defects. The objective is to quantify the influence of periodicity defects on the dispersion curves and mode shapes.

The article is structured as follows. In Section 2, localized defects are periodically introduced, and the Floquet-Bloch analysis is applied to the scale of the defects' periodicity. The numerical

verification of the existence of defect modes is presented, along with parametric studies on their eigenfrequencies regarding the amplitude of defect, and on their displacements regarding the scale of the periodicity of defects. Section 3 provides evidence for the existence of defect modes in bounded periodic media with defects. Conclusions are drawn in Section 4.

2. Floquet-Bloch analysis applied to periodic media with local defects

Introduced by Floquet [12] and then by Bloch [13], the Floquet-Bloch theory allows to reduce the size of analytical (and therefore numerical) models of a periodic medium by limiting the study to the analysis of the eigenvalues of the unit cell. This theory has been widely applied in various fields to understand the wave propagation characteristics in periodic structures, such as in solid-state physics, photonics, and acoustics.

2.1. Floquet-Bloch theory for elastic waves in periodic medium

We consider the wave equation in an infinite periodic medium of dimension d:

$$\boldsymbol{\nabla}_{\boldsymbol{x}} \cdot (\boldsymbol{C} : \boldsymbol{\varepsilon}(\boldsymbol{u})) = -\rho\omega^2 \boldsymbol{u}, \tag{1}$$

where $\boldsymbol{u}$ represents the displacement field, ω represents the angular frequency related to the frequency f, $\boldsymbol{C}$ denotes the fourth-order elasticity tensor, ρ represents the density, and $\boldsymbol{\varepsilon}(\boldsymbol{u}) = \frac{1}{2}(\nabla_{\boldsymbol{x}}\boldsymbol{u} + (\nabla_{\boldsymbol{x}}\boldsymbol{u})^{\mathrm{T}})$ is the small-strain tensor. $\nabla_{\boldsymbol{x}}(\cdot)$ denotes the spatial gradient operator and $(\cdot)^{\mathrm{T}}$ is the transposition operator. The Floquet-Bloch transform for the displacement field $\boldsymbol{u}$ is then given by:

$$\boldsymbol{u}^B(\boldsymbol{x}, \boldsymbol{k}) = \sum_{n_j \in \mathbb{Z}^{d_\mathrm{p}}} \boldsymbol{u}(\boldsymbol{x} + n_j \boldsymbol{g}_j) e^{-i\boldsymbol{k}\cdot(\boldsymbol{x} + n_j \boldsymbol{g}_j)}, \tag{2}$$

with $\{\boldsymbol{g}_j\}_{j=1,\ldots,d_\mathrm{p}}$ the basis of periodicity vectors of the considered periodic medium, $d_\mathrm{p} \leq d$ the dimension of the periodicity and $\boldsymbol{k}$ represents the wave vector. Applying the Floquet-Bloch transformation to Eq. (1), we obtain an eigenvalue problem defined on the unit cell with $\boldsymbol{k}$ belongs to the first Brillouin zone:

$$(\boldsymbol{\nabla}_{\boldsymbol{x}} + i\boldsymbol{k}) \cdot [\boldsymbol{C} : (\boldsymbol{\varepsilon}(\boldsymbol{u}^B) + \boldsymbol{u}^B \otimes_s i\boldsymbol{k})] = -\rho\omega^2 \boldsymbol{u}^B \tag{3}$$

In addition to Eq. (3), periodic boundary conditions should be imposed on the boundaries of the unit cell.

In what follows, we consider 1D and 2D periodic media with periodically induced defects so that Floquet-Bloch theory can still be used. The defects are introduced in the following way: the unit cell of the medium without defects is denoted as q_0, and the unit cell of the medium with defects $Q_0 = N \times q_0$ is composed of N q_0 cells, among which, only one differs from the others. The Floquet-Bloch theory is then applied to Q_0, allowing for the calculation of dispersion curves and corresponding modes. In the following, we call such a model a two-scale model, with q_0 the smaller scale and Q_0 the larger scale. All numerical simulations were conducted using the COMSOL Multiphysics code.

2.2. Defect modes in 1D case

In the 1D case, A cell q_0 of length l is composed of two bars of length l_1 and l_2 with different properties. A localized defect is periodically introduced in a cell q_0 either by disturbing the lengths of the two subdomains (l_1, l_2) while maintaining $l_1 + l_2 = l$; or by disturbing the Young's modulus E_1 of the subdomain l_1. In Figure 1, a two-scale model with $N = 6$, so $Q_0 = 6 \times q_0$, is presented as an example of the considered media.

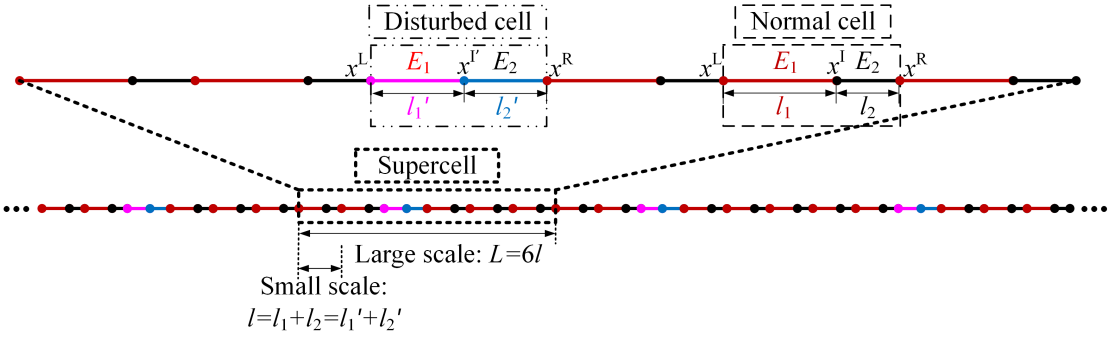

Figure 1. 1D two-scale model with $Q_0 = 6 \times q_0$ and a defect introduced on the third cell by disturbing bar's length.

Table 1. Geometry and mechanical parameters of the 1D periodic structure.

Bar	Young's modulus $E_{j(j=1,2)}$ (GPa)	Density $\rho_{j(j=1,2)}(\mathrm{kg/m^3})$	Length $l_{j(j=1,2)}(\mathrm{mm})$
1	50	2700	4
2	250	2700	1.5

The perturbation amplitudes for the bar's length and Young's modulus are defined as $\eta_l \triangleq \frac{l_2'-l_2}{l}$ and $\eta_E \triangleq \frac{E_1'-E_1}{E_1}$, respectively. In the non-disturbed model, the material and geometry parameters in Table 1 are used.

Firstly, we investigated the dispersion curves and mode shapes of two models, each with a different type of defect applied to the third q_0 cell in the Q_0 cell. These are presented alongside the dispersion curves and mode shapes of the non-disturbed model (cf. Figure 2). For the geometric defect case, we set $\eta_l = 10.8\%$, and for the material defect case, we set $\eta_E = 50\%$. Each model was analyzed for the first 24 modes, covering the first four passbands. In comparison to the non-disturbed model, defect modes (red lines) appeared inside the stop bands. The dispersion curve of the last mode is marked by triangle markers, and the 23^{rd} mode is marked by circles. The mode shapes of these two modes in the non-disturbed and disturbed models are then compared. Regardless of the type of defect, the displacement of the mode generated by the defect is localized on the disturbed q_0 cell.

To further demonstrate that the defect modes are localized at the disturbed cell, we examined three two-scale models with respectively $N = 3$, 6, and 12 while maintaining the bar length defect $\eta_l = 10.8\%$ or Young's modulus's defect $\eta_E = 50\%$ in the same small cell, as shown in Figure 3. Each two-scale model consists of N modes within each passband. For the low-frequency case, we considered the 6th mode for $N = 3$, the 12th mode for $N = 6$, and the 24th mode for $N = 12$. For the high-frequency case, we examined the 12th, 24th, and 48th modes for the three models. Regardless of the type of defect, the mode shapes are localized on the disturbed cell and converge as the number of small cells increases. The convergence is faster on higher frequencies compared to lower frequencies.

To study the influence of the amplitude of defect on the appearance and eigenfrequencies of the defect modes, a parametric study is carried out, considering the amplitude of defects η_l and η_E. The results are depicted in Figure 4, where the pass bands are represented by blue lines, determined by connecting the maximum and minimum frequencies of each eigenmode. With the increase of the amplitude of defects, mini-bandgaps appear inside each pass band. In stop bands that correspond to stop bands of the initial periodic medium without defects, the eigenfrequencies of defect modes exhibit a monotonic increase with the amplitude of the defect. Specifically, when

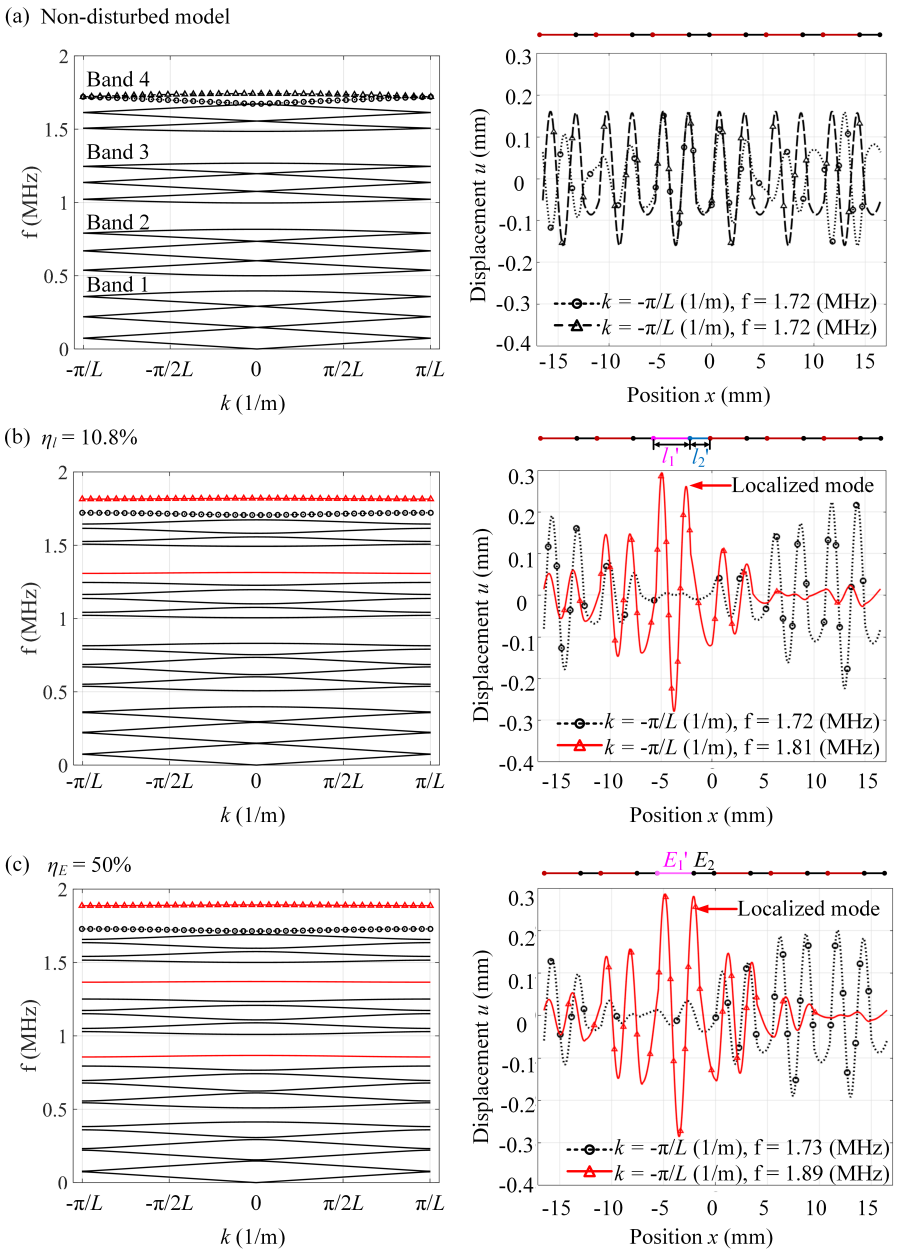

Figure 2. Dispersion curves (left) and mode shapes (right) of (a) the propagative modes (black dotted with circles and black dashed lines with triangles) in the non-disturbed medium, and the defect modes (red line with triangles) alongside the neighboring propagative mode (black dotted line with circles) of the medium with either (b) a geometric defect or (c) a material defect.

Young's modulus E_1 increases or when the bar length l_2 becomes longer, the eigenfrequencies of defect modes increase. Conversely, the eigenfrequencies of defect modes show a monotonic decrease when Young's modulus E_1 decreases or when the bar length l_2 becomes shorter.

2.3. Defect modes in 2D case

In the 2D case, the unit cell Q_0 of the medium with defects comprising 6×6 q_0 cells, i.e., N = 36. Each q_0 cell is composed of a matrix with a circular inclusion. The geometric and

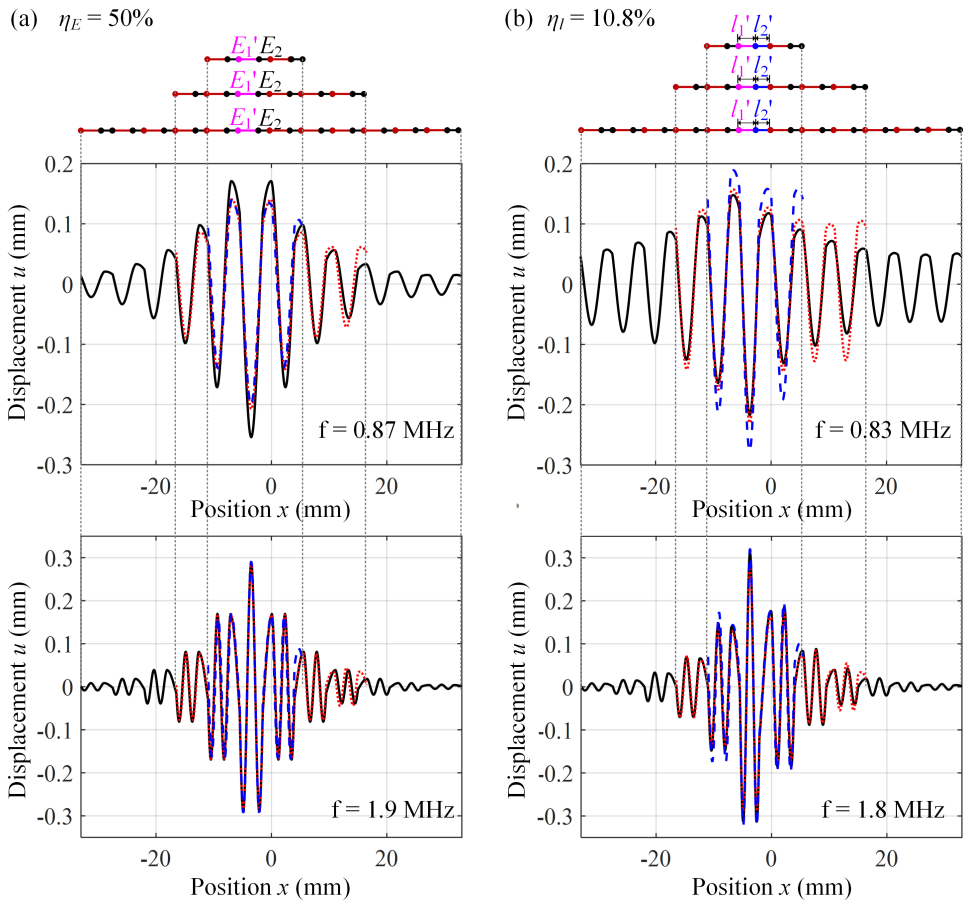

Figure 3. Mode shape of the defect modes at the same wave vector $\boldsymbol{k} = 0$ on different frequencies in different two-scale models with respectively $N = 3$, 6, and 12 with defects of (a) bar length $\eta_l = 10.8\%$ and (b) Young's modulus $\eta_E = 50\%$.

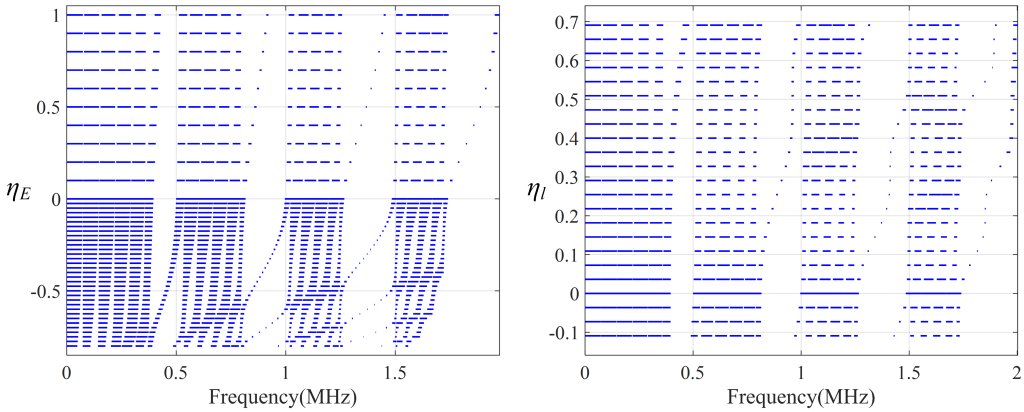

Figure 4. Influence of the amplitude of defect of bar's length (left) and of Young's modulus (right) on the pass bands (blue lines) of 1D two-scale structure.

material parameters of the non-disturbed model are summarized in Table 2. In this context, E denotes the Young's modulus, ν stands for the Poisson coefficient, and ρ represents the density. The subscript "mat" denotes parameters for the matrix, while "int" corresponds to those for the inclusion.

For the medium with defect, in the unit cell Q_0, the Young's modulus of the matrix in the central q_0 cell disturbed (Figure 5 (left)). The Floquet-Bloch theory is then applied to the unit cell Q_0, and periodicity conditions are applied to the boundaries. In the reciprocal space of the wave vector $\boldsymbol{k}$, the Brillouin zone is defined as dual to the unit cell. In Figure 5 in the middle, the gray square represents the first Brillouin zone, and the triangular region delimited by the contour Γ-X-M-Γ is the irreducible Brillouin zone, taking into account the symmetry properties of the unit cell. The vertices of this zone have coordinates: $\Gamma(0,0)$, $\mathrm{X}(\pi/L,0)$, $\mathrm{M}(\pi/L,\pi/L)$.

Table 2. Geometry and material parameters of 2D periodic structure.

L (m)	R(m)	E_{mat}(GPa)	E_{inc}(GPa)	ν_{mat}	ν_{inc}	ρ_{mat}(kg/m^3)	ρ_{inc}(kg/m^3)
0.013	0.0045	0.233	10	0.25	0.3	1750	2100

The dispersion curves are plotted regarding the contour of the irreducible Brillouin zone of the two-scale model in Figure 5 on the right. A defect mode (highlighted in red) is observed within the first band gap. The blue crosses mark the defect modes and neighboring propagative modes at points Γ ($k_1 = k_2 = 0$) and M ($k_1 = \pi/L, k_2 = \pi/L$) whose mode shapes will be studied later.

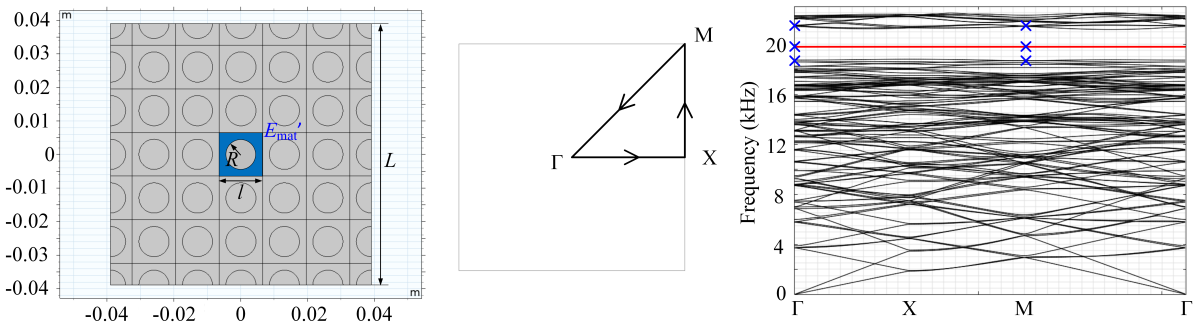

Figure 5. 2D two-scale model composed of 36 small cells with a defect of Young's modulus of the central matrix (left); the first Brillouin zone with the irreducible zone (middle); the dispersion curves of the two-scale model with the defect mode highlighted in red (right).

Figure 6 displays $||\boldsymbol{u}^B||$ for defect modes and neighboring propagative modes at points Γ and M in the medium with defects, alongside the mode shapes of the modes at the same frequencies in the non-disturbed medium for comparison. At the point Γ, the mode shape of the defect mode is quasi-isotropic and concentrated around the disturbed cell. At point M, the mode shape of the defect mode is no longer isotropic under the influence of the wave vector but remains localized around the disturbed cell.

Similar to the 1D case, in the 2D structure the defect modes remain concentrated around the disturbed cell by increasing the scale of the periodicity of introducing defects. For a two-scale model containing 8×8 small cells, the mode shape of the defect mode remains concentrated around the disturbed cell (Figure 7).

A parametric study is conducted to investigate the influence of the variation in radius $\eta_R \triangleq \frac{R'-R}{R}$ and Young's modulus $\eta_{E_{\mathrm{mat}}} \triangleq \frac{E'_{\mathrm{mat}}-E_{\mathrm{mat}}}{E_{\mathrm{mat}}}$. The results are depicted in Figure 8. As the radius of the center cell decreases, the eigenvalue of the defect mode decreases. Conversely, the eigenvalue of the defect mode increases with the Young's modulus of the matrix of the center cell.

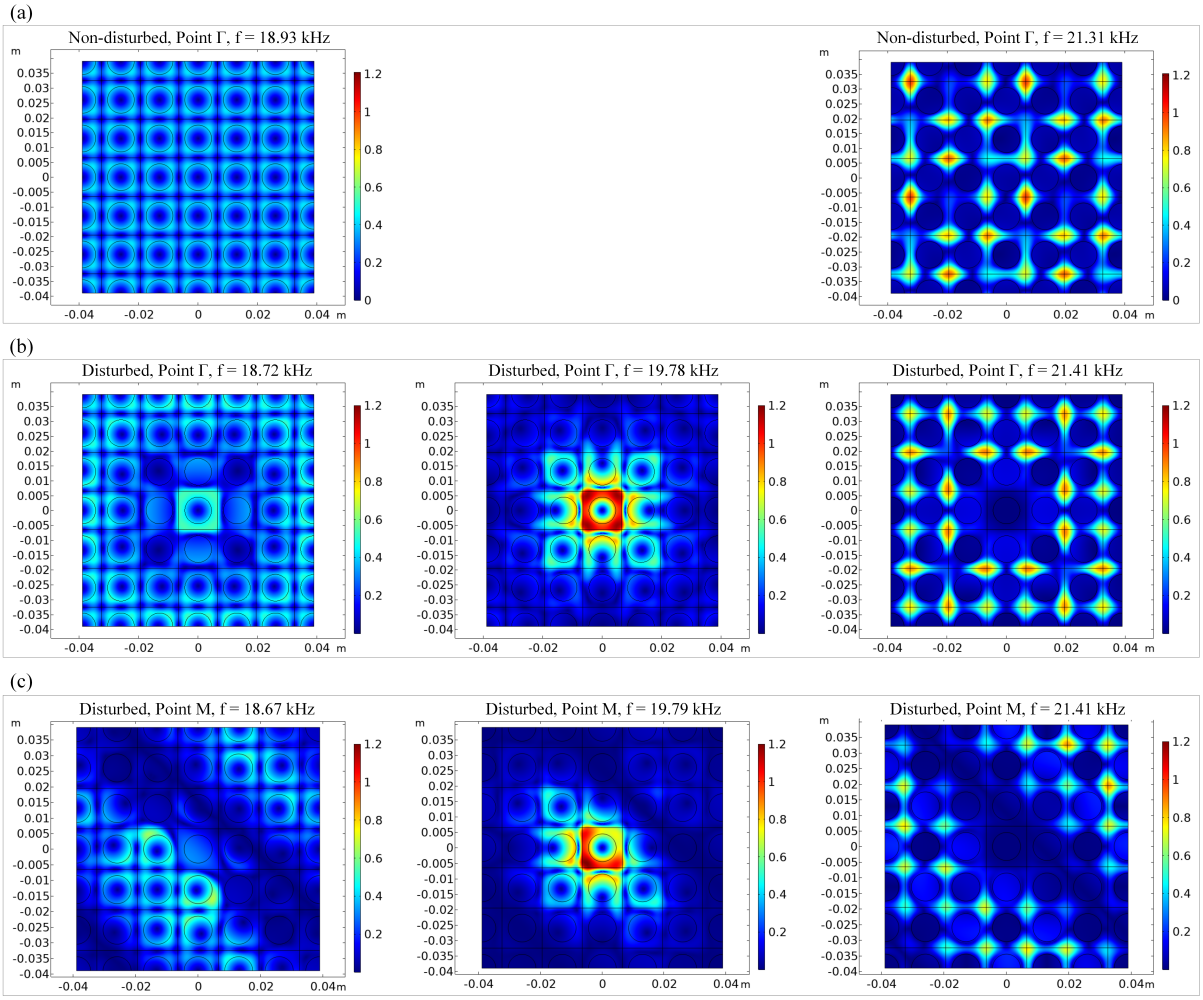

Figure 6. Comparison of mode shapes of non-disturbed and disturbed model. (a) Mode shapes $||\boldsymbol{u}^B||$ of the two propagative modes at the point Γ of the non-disturbed model; (b) mode shapes $||\boldsymbol{u}^B||$ of the defect mode (middle) and the two neighbor modes in pass band (left and right) of the disturbed model at the point Γ and (c) at the point M.

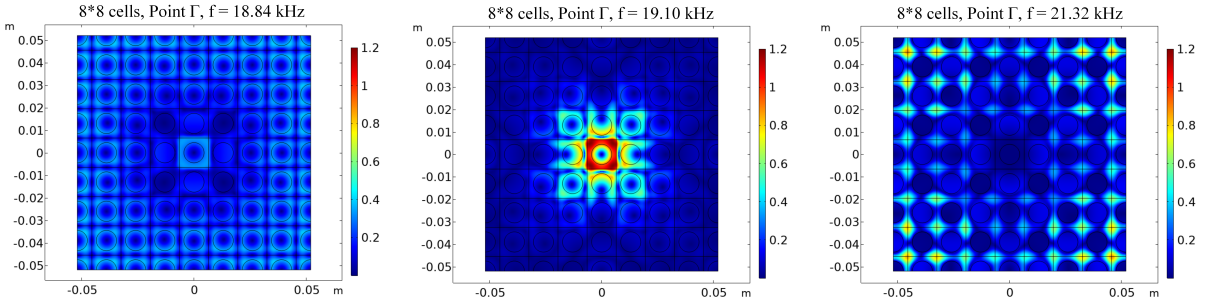

Figure 7. Mode shapes $||\boldsymbol{u}^B||$ at the point Γ of the defect mode (middle) and the two neighbor modes in pass band (left and right) for two-scale models composed of 64 small cells.

3. Numerical analysis of a bounded periodic medium with defects

The preceding section examined defects in infinite periodic media. In this section, we focus on studying defects introduced in bounded media to investigate whether the bounded nature of

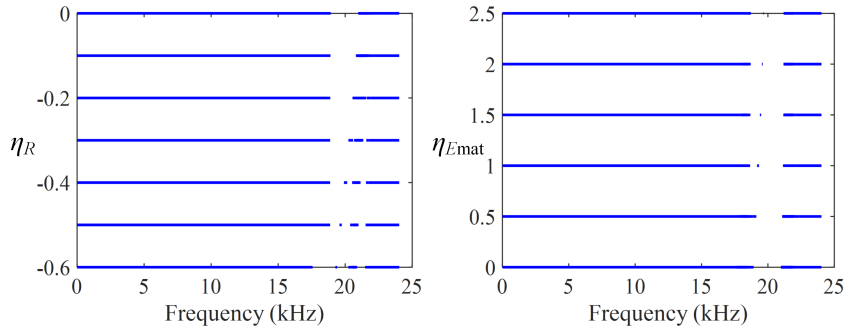

Figure 8. Impact of defect amplitude on pass bands (blue lines) in 2D two-scale structures: defect on center inclusion's radius (left) and on center matrix's Young's modulus (right)

the medium has an impact on the emergence of defect modes.

3.1. Setting of finite element models

For the study of the bounded periodic medium, the OOFE code (Object-Oriented Finite Element) [27] is employed for simulating the attenuation of the output signal and the defect modes in non-periodic models. Developed in the LMPS laboratory (Mechanical Laboratory of Paris-Saclay University), the OOFE code is specifically designed for simulating the propagation of elastic waves. It has been utilized in various research endeavors, such as the temporal simulation of a 2D matrix/inclusion periodic medium by M. Darche [28] for the verification of band gaps predicted by theoretical analysis and the simulation of ultrasonic wave propagation in polycrystal materials by X. Bai [29].

Here, the geometric and material parameters from Table 2 are used. The finite element sizes inside the inclusion and the matrix are in the order of magnitude of 2.4 mm and 0.38 mm, respectively. The time step is set as $\Delta t = 1.4 \times 10^{-7}$s, and the number of finite elements in the smallest wavelength is $N_{\text{elet}} = 15$. For all models in this section, a uniform surface pressure load is applied on the left side where the input signal is uniformly applied. A transparent boundary condition is applied on the right side of the model, and symmetric boundary conditions are applied on the top and bottom. An explicit solver based on the discontinuous Galerkin method in space is used with a CFL number set to 0.15.

The amplitude of the pressure loading is a Ricker wavelet defined as

$$R_T(t) = A\left(1 - 2\left(\pi\frac{2t-T}{T}\right)^2\right)e^{-(\pi\frac{2t-T}{T})^2}, \tag{4}$$

with A being the amplitude and T the period of the Ricker wavelet, whose frequency domain is centered at 25 kHz (Figure 10).

3.2. Verification of the existence of defect modes inside stop bands

The bounded model is created by replicating the unit cell Q_0, with $N = 5$, of the 2D two-scale model in the horizontal direction two times, resulting in 5×10 q_0 cells (Figure 10). In this context, the presence of 10 q_0 cells allows us to approximate the anticipated band gap as predicted in the infinite periodic medium [28]. We analyze the kinetic energy $E_k = \int_{q_0} \frac{1}{2}\rho(v_x^2 + v_y^2)\mathrm{d}\boldsymbol{x}$ in three q_0 cells at different positions, where v_x and v_y represent the velocity in the horizontal and vertical directions. In each small cell, the kinetic energy is calculated by doing numerical integration at 8×8 sample points. The three selected q_0 cells are located in the unit cell Q_0 2 (cf. Figure 10): the center q_0 cell (red), where a defect will be added, its right neighboring cell (green), and a q_0 cell in the corner of Q_0 (blue) the farthest from the center cell.

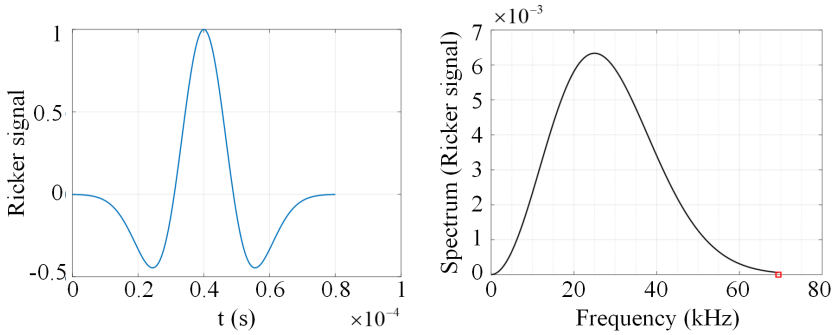

Figure 9. Ricker wavelet used for temporal loading (left) and its frequency content (right).

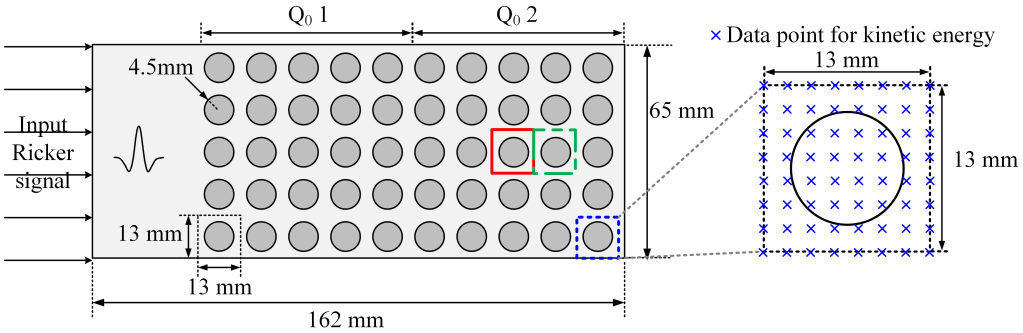

Figure 10. 2D bounded medium consisting of 5×10 small cells. On the left, three sampling cells are highlighted: the center cell (in red), the neighboring cell (in green), and the marginal cell (in blue). The right side illustrates the data points of collecting the kinetic energy in each of these cells.

In Figure 11, the gray rectangles represent the theoretical stop bands, which were obtained through COMSOL simulations of a model periodic in the horizontal direction. Each unit cell of the model comprises 5×5 small cells. The amplitudes of the kinetic energies in the three cells decrease to almost zero at the frequency of the stopbands, indicating that the bounded model effectively captures the wave attenuation behaviors of the periodic model in the horizontal direction.

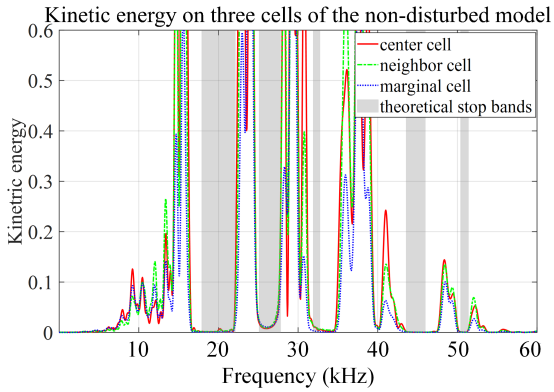

Figure 11. Capture of stop bands on the three sampling cells of the bounded periodic model

The bounded periodic model is then used to examine the impact of geometry and material

defects on wave propagation phenomena. Initially, a radius defect $\eta_R = -50\%$ is introduced to the center inclusion (Figure 12 (a)). The comparison of kinetic energy between the disturbed cell and its counterpart in the non-disturbed bounded model is illustrated in Figure 12 (b). In the disturbed cell, a pulse of kinetic energy appears at a frequency within the theoretical stop band (gray band). This theoretical stop band is obtained from simulations of a model periodic in the horizontal direction, consisting of unit cells with 5×5 small q_0 cells. The model features a radius defect of $\eta_R = -50\%$ at the center q_0 cell of each unit cell. Figure 12 (c) illustrates the comparison of kinetic energy on the three sampling q_0 cells of the disturbed model. In the neighbor cell, the energy is significantly smaller than in the defect cell, and the energy within the marginal cell is nearly zero. This demonstrates that the kinetic energy is localized around the disturbed cell, and its amplitude decreases rapidly with the increase of distance from the defect.

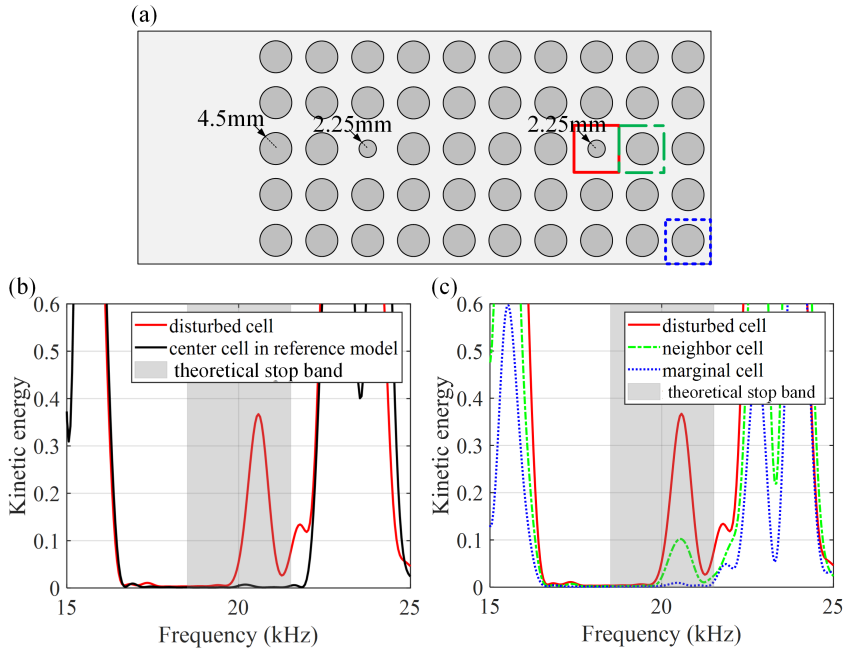

Figure 12. (a) The bounded periodic model with a radius defect $\eta_R = -50\%$. (b) Kinetic energy of the center cell in bounded disturbed model and non-disturbed model (reference model); (c) Kinetic energy on the disturbed cell, neighbor cell and marginal cell of the disturbed model with defect of radius $\eta_R = -50\%$.

Next, Young's modulus defects of $\eta_{E_{\text{mat}}} = 330\%$ are introduced in the center matrix, as illustrated in Figure 13. Regardless of the defect amplitude, a kinetic energy pulse is consistently observed within the defect cell at a frequency within the theoretical stop band. Similar to the case before, this theoretical stop band is obtained from simulations of a model periodic in the horizontal direction with a radius defect of $\eta_R = -50\%$ at the center q_0 cell of each unit cell. The amplitude of this pulse diminishes rapidly with distance from the defect.

4. Conclusions and perspectives

This paper presents a series of numerical simulations to qualitatively characterize the influence of defects on eigenfrequencies and mode shapes of imperfect periodic media. The presence of defect modes inside the stop bands of periodic media is illustrated, and their mode shapes are analyzed through numerical simulation. The deformation of the defect mode is localized around the disturbed cell, and their eigenfrequencies exhibit a monotonic variation with the amplitude

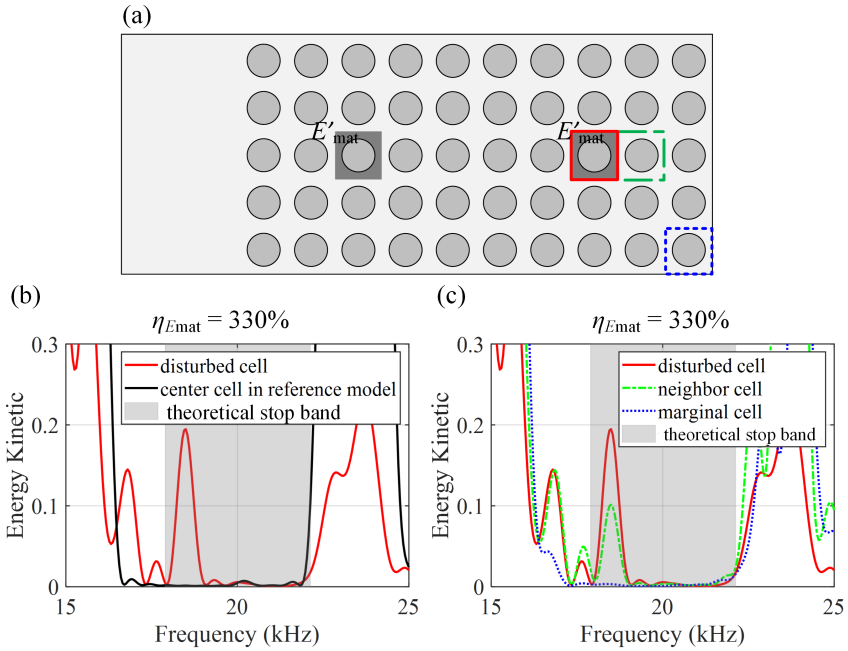

Figure 13. (a) The bounded periodic model with a radius defect $\eta_{E_{\text{mat}}} = 330\%$. (b) Kinetic energy of the center cell in disturbed model and non-disturbed model (reference model); (c) Kinetic energy on the disturbed cell, neighbor cell and marginal cell of the disturbed model with defect of Young's modulus $\eta_{E_{\text{mat}}} = 330\%$.

of the defects. Additionally, the appearance of defect modes is observed within bounded periodic media featuring defects.

References

[1] Li Z, Wang Z, Guo Z, Wang X and Liang X 2021 *Applied Physics Letters* **118** 161903

[2] Sheng P, Fang X, Wen J and Yu D 2021 *Journal of Sound and Vibration* **492** 115739

[3] Weiner M, Ni X, Li M, Alù A and Khanikaev A B 2020 *Science Advances* **6** eaay4166

[4] Li Y, Pan F, Lin X, Yang K, Ren Y, Yang W and Chen Y 2023 *International Journal of Mechanical Sciences* **243** 108044

[5] Rupin M, Lemoult F, Lerosey G and Roux P 2014 *Physical review letters* **112** 234301

[6] Zhou X, Fu Q H, Zhao J, Yang Y and Zhao X P 2006 *Optics express* **14** 7188–7197

[7] Lim C 2022 *Archives of Computational Methods in Engineering* **29** 1137–1198

[8] Vasileiadis T, Varghese J, Babacic V, Gomis-Bresco J, Navarro Urrios D and Graczykowski B 2021 *Journal of Applied Physics* **129** 160901

[9] Tian Z, Shen C, Li J, Reit E, Bachman H, Socolar J E, Cummer S A and Jun Huang T 2020 *Nature communications* **11** 762

[10] Liu J, Guo H and Wang T 2020 *Crystals* **10** 305

[11] De Ponti J, Paderno N, Ardito R, Braghin F and Corigliano A 2019 *Applied Physics Letters* **115** 031901

[12] Floquet G 1883 *Annales scientifiques de l'École normale supérieure* vol 12 pp 47–88

[13] Bloch F 1929 *Zeitschrift für physik* **52** 555–600

[14] Shahraki D P and Guzina B B 2022 *International Journal of Solids and Structures* **234** 111239

[15] Karličić D, Cajić M, Paunović S and Adhikari S 2021 *Mechanical Systems and Signal Processing* **155** 107591

[16] Vila J, Pal R K, Ruzzene M and Trainiti G 2017 *Journal of Sound and Vibration* **406** 363–377

[17] Farzbod F and Leamy M J 2009 *Journal of Sound and Vibration* **325** 545–551

[18] Suo Y, Wang B, Jia P and Gong Y 2020 *Materials Today Communications* **25** 101663

[19] Fayazbakhsh K, Movahedi M and Kalman J 2019 *Materials Today Communications* **18** 140–148

[20] Mukhopadhyay T and Adhikari S 2017 *Composite Structures* **162** 85–97

[21] Denry I 2013 *Dental materials* **29** 85–96

[22] Yuan T, Kuo W and Bae S J 2011 *IEEE Transactions on Semiconductor Manufacturing* **24** 392–403

[23] Wilby A and Neale D 2009 *Mater. Sci. Eng* **3** 48–75

[24] DeHon A and Naeimi H 2005 *IEEE Design & Test of Computers* **22** 306–315

[25] Bouzit D and Pierre C 1995 *Journal of Sound and Vibration* **187** 625–648

[26] Ding L, Zhu H P and Wu Q y 2019 *Journal of Engineering Mechanics* **145** 04019093

[27] Tie B, Mouronval A S, Nguyen V D, Series L and Aubry D 2018 *Computer Methods in Applied Mechanics and Engineering* **338** 299–332

[28] Darche M, Lopez-Caballero F and Tie B 2023 *Journal of Sound and Vibration* 118158

[29] Bai X, Tie B, Schmitt J H and Aubry D 2018 *Ultrasonics* **87** 182–202